JOURNAL OF SOLID STATE CHEMISTRY 68, 28–37 (1987)

Photoelectrochemical Characterization of Several Semiconducting Compounds of Palladium with Sulfur and/or Phosphorus

J. C. W. FOLMER,* J. A. TURNER, AND B. A. PARKINSON†

Photoconversion Research Branch, Solar Energy Research Institute, 1617 Cole Boulevard, Golden, Colorado 80401

Received February 13, 1985; in revised form June 18, 1986

Semiconducting compounds of palladium with sulfur and/or phosphorus were prepared as crystals and their semiconducting and photoelectrochemical properties studied. The compounds include PdS, PdPS, $Pd_3(PS_4)_2$, and PdP_2 and crystal growth was accomplished by chemical vapor transport with halogens and Bridgeman methods. Photoelectrochemical techniques were used to measure bandgap, transition type, doping level, majority carrier type, flatband potential, quantum yield for electron flow, and stability in a photoelectrochemical cell. The previously undetermined bandgap of PdP_2 is reported (1.08 eV, indirect). © 1987 Academic Press, Inc.

Introduction

Photoelectrochemical cells have demonstrated high-energy conversion efficiencies both in regenerative photovoltaic and in photoelectrolysis devices (*1, 2*). In most cases of efficient energy conversion, conventional semiconductor materials were used (i.e., Si, III–V's and II–VI's), primarily because of their high state of development for solid state applications and their commercial availability. In many cases the semiconductor electrode can be used without modification; this is particularly true for regenerative systems where there is a specific interaction (e.g., specific adsorption) at the electrode/electrolyte interface. In other cases, however, catalysts must be placed on the surface in order to obtain good kinetic behavior. This is particularly true for water-splitting reactions. For efficient hydrogen evolution from p-InP, for example, noble metal catalyst islands were deposited whereas the unmodified surface showed poor kinetic behavior (*3, 4*). The high efficiencies and stabilities achieved by the aforementioned systems have not been matched for photoreactions proceeding through more kinetically difficult multielectron (or hole) transfer reactions. These reactions, which are of particular interest for solar energy conversion, include O_2 evolution from water, N_2 reduction to ammonia, and CO_2 reduction to formate, fomaldehyde, and methanol. Attempts to modify the surfaces of conventional semiconductors with catalysts to promote these processes have met with limited success (*5–7*). Another approach is to use a mediator coupled to a homogeneous catalyst; for exam-

* Present address: Dow Chemical (Nederland) BV, Analytical Development Department, P.O. Box 48 4530 AA, Terneuzen, The Netherlands.

† Present address: Central Research and Development Department, Experimental Station E328/105, E. I. DuPont de Nemours, Inc., Wilmington, DE 19898.

0022-4596/87 $3.00

ple, recently methyl viologen was used to mediate an enzyme catalyst to promote the uphill photoreduction of CO_2 to formic acid (*8*).

Another approach is to try to combine semiconductivity and catalytic properties in a single material. Tributsch and his group have used this approach to develop materials based on RuS_2 for the photooxidation of water (*9, 10*). Our approach is to extend the study of the semiconducting chalcogenides and pnictides of the Group VIII metals to investigate the concept of catalytic photoelectrodes. In this report we will discuss some aspects of the Pd–P–S ternary system. Apart from their crystallographic structures, little is known of these phases. None of these materials have been studied previously in the photoelectrochemical context although Wold *et al.* have reported on the photoelectrochemistry of PdPSe (*11*). More directly related, first row Group VIII, thiophosphates ($NiPS_3$, $CoPS_3$, $FePS_3$) have also been studied as photoelectrodes (*12*).

Preparation

The Pd–P–S system has been studied mainly by high-pressure techniques by Bither *et al.* (*13*). Crystal growth of a related compound, PdPSe, by vapor transport has been reported (*11*). In our study both vapor transport and melting techniques were used to obtain crystals of the various Pd–P–S phases. Fused quartz ampoules were used either in three-zone furnaces (Lindberg) or in a programmable temperature-controlled muffle furnace. We attempted the vapor transport growth of PdS_2 by adding Cl_2, a small excess of sulfur, and either P or Al to the ampoule. Instead of PdS_2, crystals of PdS were obtained. Following the recipe for crystal growth of PtS_2 (*14*), we obtained a solid mass of purplish red crystals of $Pd_3(PS_4)_2$, which were transported to the cooler end of an ampoule loaded with Pd, P, and S in the ratio 1 : 1 : 3 (Cl_2; 760–740°C). A few intergrown small crystals of PdPS were also obtained in this experiment. Although this indicates that Cl_2 transport of PdPS is possible, transport of this material when an ampoule was loaded with a slight excess of P and S above the nominal PdPS composition was not observed.

At higher temperatures (930°C), the formation of a melt was observed. Upon removal from the furnace, a string of bladelike crystals of PdPS together with an unidentified ingot were obtained. The crystals were up to 3–4 mm long and up to 1 mm wide. They were very thin, as indicated by microscopic examination of some crystals which showed a reddish translucence. These crystals (grown in the presence of chlorine) were the most suitable for PEC investigation. Most of the measurements reported herein on PdPS were obtained with those crystals. To study the melting behavior of PdPS, we heated samples, with 1 : 1 : 2 composition with no added Cl_2, to a temperature of ca. 950°C and cooled slowly. Despite placing the ampoule vertically in the furnace, the material grew to the top of the ampoule (~20 cm) in unusual serpentine strings of small intergrown bladelike crystals. We expected a second phase to be present with which PdPS would be in a solvent/solute relationship since this behavior resembles growth through capillary action. X-ray diffraction revealed only PdPS lines, indicating that the melting of the material is essentially congruent. Note, however, that volatile P/S components usually condense on the contents of the ampoules in the form of yellow-orange sublimates. These sublimates reflect the rather dense phosphorus/sulfur-containing atmosphere at higher temperatures. (Care must be taken when opening the ampoules because these P/S materials hydrolyze upon exposure to air, evolving noxious fumes.) CH_3OH, CS_2, and sometimes dilute HNO_3

were used to clean the crystals. It appears that proper control of the P/S pressures is vital for control of the PdPS melting process. A detailed study of the Pd–P–S phase diagram including the pressure dependencies would be desirable but is beyond the scope of this paper.

Attempts to grow crystals of PdP_2 by vapor transport (Cl_2, Br_2) and flux growth (Sn, Bi, Te) were unsuccessful. Cone-shaped crystals of this phase were obtained when PdPS was heated to 970°C with the addition of a large amount of excess P relative to S, thus reemphasizing the above statement concerning the phase diagram. A summary of the phases investigated in this study and their crystal structures and the techniques used to obtain crystals is shown in Table I.

Experimental

Materials obtained were identified by powder X-ray diffractometry. Energy-dispersive electron beam-induced X-ray spectroscopy (EDAX microprobe) was also used to verify the composition of the crystals.

Electrodes were constructed from suitable crystals (down to <1 mm in size) by mounting them on a copper plate wetted with In–Ga eutectic and insulating all but the desired crystal face with epoxy (Epoxy-Patch, Dexter Corp.). All materials studied were *n*-type. Photoelectrochemical measurements encompassed:

(*1*) *Current–voltage curves.* Current–voltage behavior was studied in the dark and under illumination using an EG&G Potentiostat and a tungsten–halogen light source. Counter electrodes were Pt and, if used, reference electrodes were saturated calomel electrodes (SCE, 0.242 V with respect to the NHE). In some cases light chopping and a lock-in amplifier were used to separate the photocurrent from dark currents.

(*2*) Photocurrent spectroscopy. A computer-controlled system consisting of a monochromator, a potentiostat, a light source, a chopper, and a lock-in amplifier was used. Band gap analysis was performed by plotting $(h\nu \times \text{response})^n$ vs $h\nu$ with $n = 2$ or $\frac{1}{2}$, for direct and indirect gaps, respectively, (*19*). Care was taken to avoid distortions of the spectra by photoconductive or solution absorption effects.

Absolute quantum yields were obtained by constraining and positioning the monochromator beam until it was incident exclusively on the crystal and then measuring the photon flux at a convenient wavelength and subsequently scaling the response with this value.

(*3*) *Capacitance–voltage.* Mott–Schottky plots were obtained by measuring the phase shift of an applied ac signal on the

TABLE I

STRUCTURE AND CRYSTAL GROWTH TECHNIQUES FOR PALLADIUM-CONTAINING SEMICONDUCTORS

Compound	Structure	X-bonding	Reference	Crystal growth
PdS	Cooperite	S^{2-}	*13, 15*	CVT[a](Cl_2)
PdS_2	Layered pyrite	$(S_2)^{2-}$	*16*	Not made
PdPS	Two pyrite layers	$(S–P–P–S)^{4-}$	*13, 17*	CVT[a] + melt
PdP_2	∞ pyrite layers	$(–P–P–P–P–)_n^{-4n}$	*18*	Decomposition of PdPS
$Pd_3(PS_4)_2$	Sandwich	$(PS_4)^{3-}$	*13*	CVT (Cl_2)

[a] CVT = chemical vapor transport.

cell in the dark. Various frequencies were used to study the dispersion of the response with frequency. In all cases dispersion was observed either of the parallel kind or of the angular type (*20*). The first is characterized by a parallel shift in the linear part in the plot of C^{-2} vs voltage indicative of a shift of the flatband potential with frequency. In the second case, the intercept with the voltage axis stays approximately constant, but the slope of the line changes, indicating an apparent change in the doping level of the material with frequency. This can be interpreted as evidence for the presence of charge carriers at the surface in surface states that communicate with the bulk on various time scales. Since no data are available on the static dielectric constants (ε) for these materials, we used an arbitrary value of 10 when analyzing the Mott–Schottky data to determine the doping density. Fortunately, the value of N_d (doping level) is relatively insensitive to variations in the dielectric constant.

Electrolytes and acid cleaning and etching solutions were prepared from analytical grade reagents and were used as received. Water was purified with a Millipore water purification system with a final UV irradiation for the oxidation of organic impurities.

Results and Discussion

PdPS

The most intriguing results in the Pd–P–S system were obtained with crystals of this phase. A number of redox couples and electrolytes (all aqueous) were used to investigate its PEC behavior: Fe^{2+}, Fe(II)EDTA, CN^-, I^-, pH 8.8 phosphate buffer, $Ru(CH)_6^{4-}$, and $Fe(CN)_6^{4-}$. The photocurrent in all but the last solution was either small and unstable, or not observed. In a number of cases, e.g., I^-, clear signs of corrosion (surface pitting) were observed by microscopic inspection of the surface after the photoelectrochemical experiment. It should be noted that this contrasts sharply with the apparent stability of the homolog PdPSe in iodide as reported in the literature (*14*).

In a 0.1 *M* $K_4Fe(CN)_6$ solution, the current–voltage curves show substantial improvements with time. As is shown in Fig. 1 the photocurrent is initially rather small but scanning the potential 0.4 V either side of the short circuit potential gradually improves the magnitude of the photocurrent and the fill factor. The open circuit photopotential also increases from values less than 100 mV to over 300 mV. Similar improvements are also noted from potentiostating at positive potentials (0.2 to 0.6 V vs the solution or short circuit potential).

Figure 2 shows the time and charge evolution of light and dark currents of a PdPS crystal (A) with an area of 0.6 mm^2 in an extended test (note the logarithmic time axis). The eventual slight degradation of the photoeffect is not necessarily associated

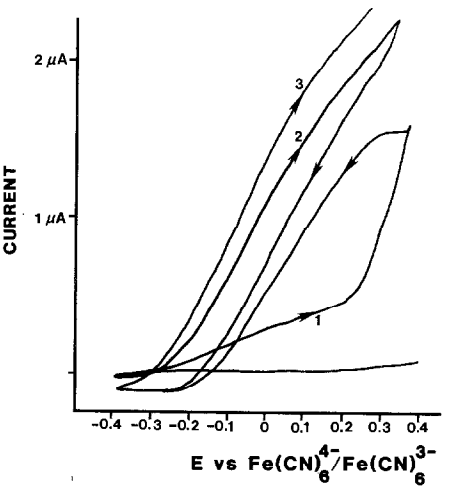

FIG. 1. The current–voltage characteristics of a two-electrode system containing a virgin PdPS sample (A) in a 0.1 *M* $K_4Fe(CN)_6$ (pH 8.8 phosphate buffer) solution. The numbers designate the scan number under illumination. Zero volts indicates the solution potential; *n*-type photovoltages are then negative with respect to zero.

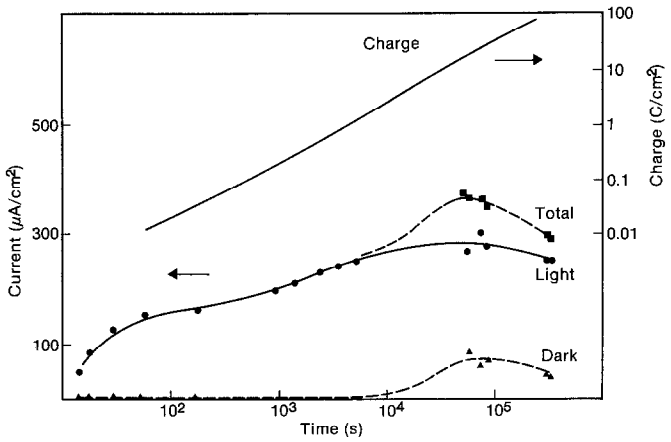

FIG. 2. The evolution with time of the current in the dark and under illumination of crystal A (cf. Fig. 1). The total charge passed through the interface in coulombs is plotted as a solid line. Note the logarithmic nature of both charge and time scales. (The total time scale of the experiment is 3 days.)

with the degradation of the crystal since some solution decomposition was observed. Iron cyanide complexes are known to be unstable toward hydrolysis and photolysis. The eventual improved (henceforth called "ameliorated") behavior indicates that the bulk semiconductor properties probably do not limit this material's performance as a photoelectrode. Microscopic inspection of the electrode surface did not reveal any signs of corrosion. Knowing that 100 C/cm^2 were passed and assuming a worst-case oxidative corrosion pathway

$$8H_2O + PdPS + 13h^+ \rightarrow Pd^{2+} + PO_4^{3-} + SO_4^{2-} + 16H^+, \quad (1)$$

we calculate that at least 40 μm should have been removed from the entire surface of the crystal if the current was entirely due to corrosion. This amount of corrosion would have been readily apparent by microscopic examination, especially considering the thinness of the crystal (~100–200 μm). The remarkable chemical interaction between the ferrocyanide and the PdPS crystal surface is discussed elsewhere in more detail (*21*).

Figures 3 and 4 show the photocurrent spectrum of crystal B and the analysis of the band edge, respectively. The analysis indicates the presence of an indirect gap at 1.45 eV followed by a direct gap at 1.66 eV. The first value is larger than the value of 1.38 eV determined with optical absorption (*13*), but compares well with our diffuse reflectance data which show an onset of reflectivity at 1.48 eV. The value is, as expected, somewhat larger than the value of 1.28 eV reported for the indirect gap of isostructural PdPSe (*11*). Measurement of the quantum yield on crystal B gave different

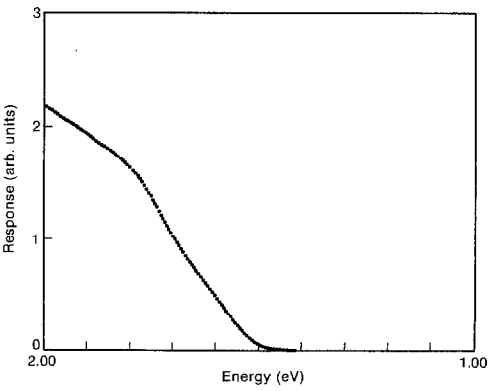

FIG. 3. Photocurrent spectrum of PdPS (B) in 0.1 *M* $K_4Fe(CN)_6$ solution.

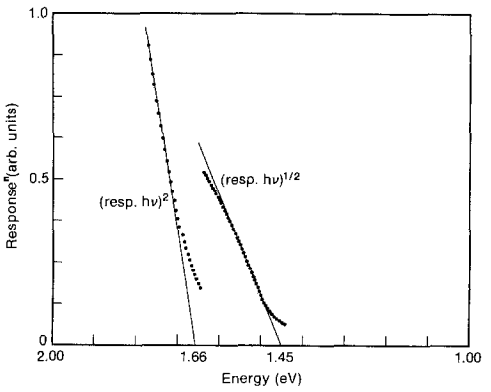

FIG. 4. Power law analysis of the photocurrent spectrum shown in Fig. 3.

values depending on the position of the beam on the electrode surface. In one experiment, we measured the monochromatic quantum yield (632.8 nm) by positioning the focused laser beam to find the spot on the surface with the highest photocurrent. In this way a monochromatic quantum yield of 0.14 was calculated for this particular spot. We should note that in all these measurements we first allowed the electrode to ameliorate its performance through exposure to $Fe(CN)_6^{4-}$ as described above.

Capacitance–voltage data (Mott–Schottky) were measured on a virgin crystal (C) in phosphate buffer. The crystal was subsequently ameliorated in ferrocyanide and the measurement was repeated in the latter solution. The data, shown in Fig. 5, indicate that the surface has acquired a negatively charged species in the amelioration process. This is shown by a shift of the flatband potential toward more negative potentials. The intercept shifts from about −0.8 V to ca. −1.0 V vs SCE. Although there is little hysteresis with potential scan direction and linearity is exhibited over a sufficiently broad voltage range, the plots do exhibit frequency dispersion. This dispersion is mainly of the angular type although the intercept (and thus flatband potential) is also somewhat affected. Assuming a static dielectric constant of 10, we arrive at an approximate doping level of 10^{17} cm^{-3}. The frequency dispersion is not surprising in view of the observation of steps on the surface. The source of dispersion is probably the presence of band gap states associated with these surface features; they may communicate rather sluggishly with the bulk and may or may not be observed at some measurement frequencies.

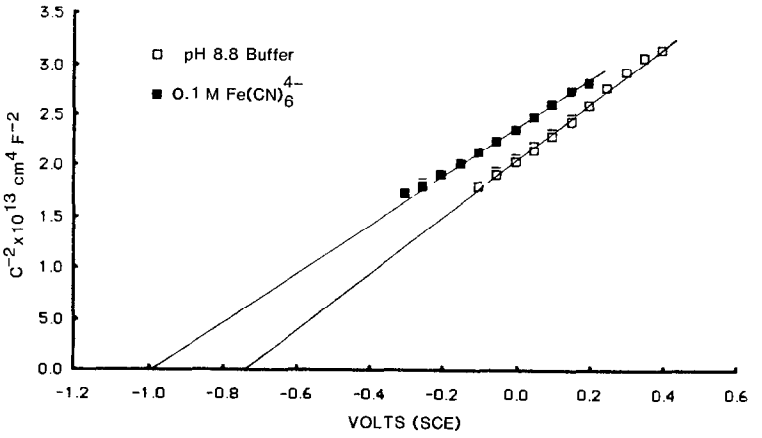

FIG. 5. Capacitance (Mott–Schottky) data before and after amelioration in ferrocyanide of the same PdPS crystal (C). Open squares are the electrode in 0.1 *M* pH 8.8 phosphate buffer. The dark squares are after 0.1 *M* $K_4Fe(CN)_6$ was added to the electrolyte.

PdP_2

Current–voltage curves of illuminated and nonilluminated crystals of this compound in polysulfide and ferrocyanide solutions revealed minimal photoeffects. The photoresponse spectrum for PdP_2 in S^{2-}/S_n^{2-} in D_2O is shown in Fig. 6. Analysis of the band edge (Fig. 7) reveals that there is a direct gap at 1.11 eV, possibly preceded by an indirect gap at 0.99 eV. D_2O was used instead of H_2O because of the IR absorption of the latter around 950 and 1100 nm. Initially, Mott–Schottky plots in pH 8.8 phosphate buffer were linear but after repeated measurements the slope decreased, indicating that the surface of the material becomes more and more degenerate. Etching the crystal in Br_2/methanol, HNO_3, HCl, aqua regia, or concentrated NaOH solution accelerated the degradation process. After the experiments the crystals appeared more blackish in color with the surface showing a golden metallic hue, indicating that the surface of this material is chemically altered by the immersion and illumination in electrolyte solutions. Amelioration effects in $Fe(CN)_6^{-4}$ solutions were not observed on this compound.

PdS

Although electrodes of this material show the blocking behavior to current flow typical of a semiconductor, very small photocurrents near the detection limit of our lock-in amplifier were observed. The photoresponse decreased to the noise level at about 2 eV so this may be taken as an upper limit for the band gap of PdS. The metallic color of the crystals (which is reminiscent of FeS_2-pyrite) indicates that the band gap is probably smaller than 2 eV. Mott–Schottky data showed good linear behavior with a frequency dispersion of the parallel type and as a result the doping density of ca. 10^{18} is more trustworthy than the V_{fb} values that range from −1.3 to −1.6 V (SCE). Because of the small photoeffects no further studies of this material were undertaken.

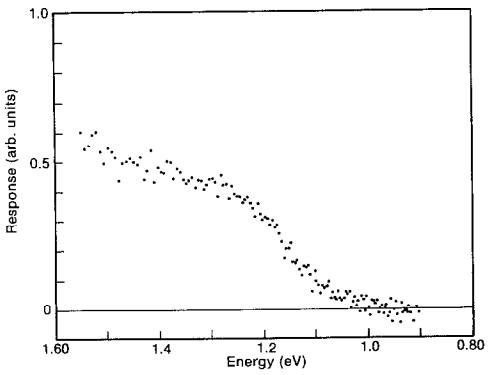

FIG. 6. The photocurrent spectrum of PdP_2 in 1 *M* NaS^{2-}/S_2^{2-} solution in D_2O.

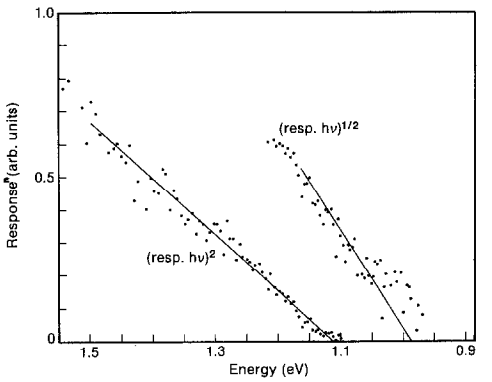

FIG. 7. Analysis plots of [response × $h\nu$]^n for $n = \frac{1}{2}$ and 2 of the response shown in Fig. 6 (PdP_2). A direct gap of 1.11 eV can be derived, possibly preceded by an indirect gap at 0.99 eV.

$Pd_3(PS_4)_2$

This material, which has an interesting layer structure (Fig. 8) (*13*), shows appreciable photoeffects in a number of solutions. The best results were obtained in I^- and Br^- electrolytes. Photocurrents decaying with time were observed in ferrocyanide solutions, a behavior contrasting to the PdPS case. Figure 9 shows light and dark curves in a 0.1 *M* Br^- solution and Fig. 10 shows the photocurrent response spectrum

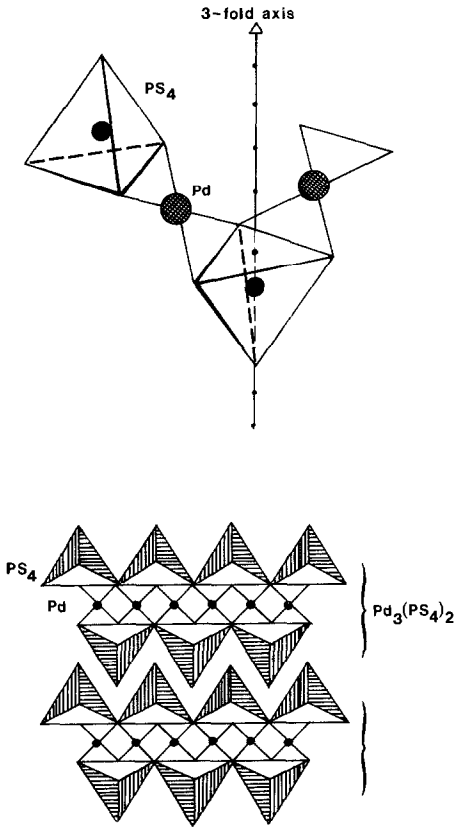

FIG. 8. The structure of $Pd_3(PS_4)_2$. Pd is coordinated in a square planar fashion by the sulfur members of two PS_4 tetrahedra. The arrangement is such that the Pd atoms form a layer sandwiched between two (PS_4) layers. The interaction across the van der Waals gap is rather weak, although there may be some interaction of the apex sulfur atom of the PS_4 unit of one layer with the Pd of the next. The bottom drawing schematically shows the peculiar interlocked layer structure that results.

in 1 *M* NaBr. Analysis of the band edge (Fig. 11) yields a value of 2.54 eV for the band gap (indirect); there is also an indication of a direct gap at 2.89 eV. A quantum yield of about 1% at 3.1 eV was measured.

The small quantum yield and the large difference between the onset of optical absorption and the photoelectrochemically measured indirect transition can be ascribed to the low mobility (or short minority carrier diffusion lengths) of carriers in this material. This is not surprising when the physical and electronic structure of the material is considered. The palladium atoms in one layer are particularly isolated from palladium atoms on an adjacent layer. This will probably limit the dispersion of the Pd-*d* band in the *c*-direction. The result is that carriers created deeply in the material, from wavelengths near the absorption edge, cannot be collected at the interface.

A $Pd_3(PS_4)_2$ electrode was illuminated under short circuit condition in a deoxygenated 1 *M* NaOH solution to test for the ability to photocatalyze the evolution of oxygen. No oxygen bubbles were observed nor was an O_2 signal measurable with a Clark electrode. After extended illumination (8 hr) photodissolution of the material was observed. The inability to observe the degradation in a short time can be understood when the most demanding photocorrosion reaction is considered (Eq. (1)).

$$40H_2O + Pd_3(PS_4)_2 + 64h^+ \rightarrow 3Pd^{2+} + 2PO_4^{3-} + 8SO_4^{2-} + 80H^+. \quad (2)$$

The photocurrents for the oxidation of bromide or halide appear to be more stable and, considering the number of holes per equivalent of $Pd_3(PS_4)_2$ dissolved (64), the

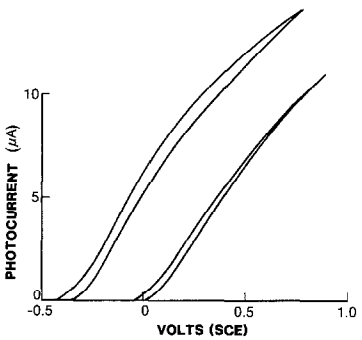

FIG. 9. The photocurrent voltage characteristics of $Pd_3(PS_4)_2$ in 0.1 *M* NaI (left curve) and 0.1 *M* Br (right curve).

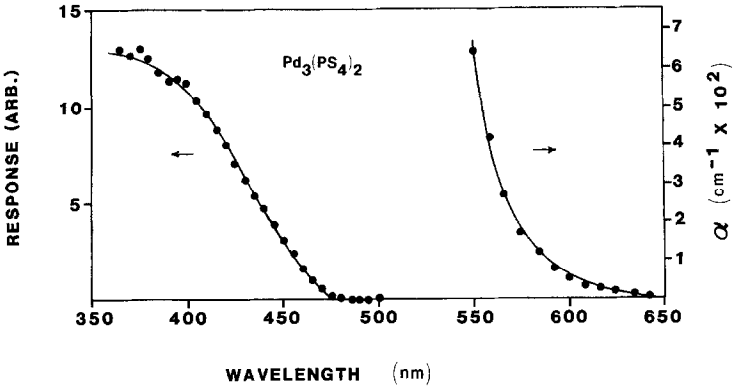

FIG. 10. The photocurrent spectrum of $Pd_3(PS_4)_2$ in 1 *M* NaBr.

determination of the actual stability of this system could take a very long time, especially if the coulombic efficiency of the photocorrosion process is less than 10%.

Conclusion

In this study we have synthesized, grown crystals, and photoelectrochemically investigated compounds of the Pd–P–S ternary system. Photoelectrochemistry has proven to be a valuable tool for the determination of a variety of semiconductor parameters such as band gap, doping level, quantum yield for electron flow, and the energy position of the bands (see Table II). Several of these values were unknown prior to this study (i.e., the band gap of PdP_2).

The long range goal of this project is to identify the catalytic reactivity of Group VIII semiconducting compounds toward reactions of interest for solar energy conversion. The screening of these and other related compounds for reactivity in the water splitting reaction and for the reduction of CO_2 or N_2 is currently in progress in our laboratory. We are encouraged by our discovery of the specific interaction of ferrocyanide with the surface sites of PdPS (*21*). Interactions of this type may be a model for the types of interactions with the semiconductor surface which would be required for multielectron transfer steps. Multiple electron transfer steps are the key step in any efficient oxidation of water to O_2 or N_2 to useful fuels or chemicals.

TABLE II

PROPERTIES OF PALLADIUM-CONTAINING SEMICONDUCTORS MEASURED WITH PHOTOELECTROCHEMICAL TECHNIQUES

Compound	E_g(PEC)	E_g(OPT)	Y_{fb}	Doping	ϕ
PdS	2.14	—	−1.5	n–5 × 10^{18}	Small
PdPS	1.45*i*, 1.66*d*	1.38	−0.8	n–10^{17}	0.14(638.2)
PdP_2	1.08*i*	?	−1.0	n–?	Small
$Pd_3(PS_4)_2$	2.61*i*	2.15	−1.0	n–10^{15}	0.02–0.1

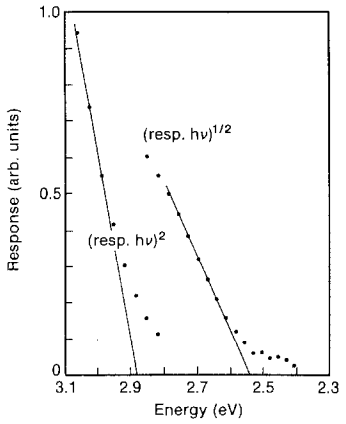

FIG. 11. Analysis plots of the photoresponse of $[Pd_3(PS_4)_2]$ (response $\times h\nu)^n$ yields a straight line for $n = \frac{1}{2}$, indicating an indirect edge at 1.54 eV; there is also possibly a direct group at 2.89 eV.

Acknowledgments

We acknowledge Dr. Jim Gude of the U.S. Geological Survey and Don Williamson of the Colorado School of Mines for the use of X-ray facilities. Chuck Herrington provided electron microprobe analysis and Fritz Franzen provided helpful discussions and the use of his laboratory facilities. Art Frank assisted with the low level oxygen detection experiments. This work was supported by the Advanced Energy Projects Division of the Office of Energy Research, U.S. Department of Energy.

References

1. B. A. PARKINSON, *J. Chem. Ed.* **60,** 338 (1983), and references therein.
2. B. A. PARKINSON, *Acc. Chem. Res.* **17,** 431 (1984), and references therein.
3. (a) E. AHRON-SHALOM AND A. HELLER, *J. Electrochem. Soc.* **129,** 2865 (1982); (b) A. HELLER AND R. G. VADIMSKY, *Phys. Rev. Lett.* **46,** 1153 (1981).
4. C. LEVY-CLEMENT, A. HELLER, W. A. BONNER, AND B. A. PARKINSON, *J. Electrochem. Soc.* **129,** 1701 (1982).
5. (a) A. J. FRANK AND K. HONDA, *J. Phys. Chem.* **86,** 1933 (1982); (b) A. J. FRANK AND K. HONDA, *J. Electroanal. Chem.* **150,** 673 (1983).
6. D. L. DU BOIS AND J. A. TURNER, *J. Amer. Chem. Soc.* **104,** 4989 (1982).
7. S. GRAYER AND M. HALMAN, *J. Electroanal. Chem.* **170,** 363 (1984).
8. B. A. PARKINSON AND P. F. WEAVER, *Nature (London)* **309,** 148 (1984).
9. H. M. KUHNE AND H. TRIBUTSCH, *J. Electrochem. Soc.* **130,** 1448 (1983).
10. H. M. KUHNE AND H. TRIBUTSCH, *Ber. Bunsen Ges. Phys. Chem.* **88,** 19 (1984).
11. J. V. MARZIK, R. KERSHAW, K. DWIGHT, AND A. WOLD, *J. Solid State Chem.* **44,** 382 (1982).
12. C. E. BYVIK, B. T. SMITH, AND B. REICHMAN, *Sol. Energy Mater.* **7,** 213 (1982).
13. T. A. BITHER, P. C. DONOHUE, AND H. S. YOUNG, *J. Solid State Chem.* **3,** 300 (1971).
14. A. FINLEY, D. SCHLEICH, J. ACKERMANN, S. SOLED, AND A. WOLD, *Mater. Res. Bull.* **9,** 1655 (1974).
15. A. F. WELLS, "Structural Inorganic Chemistry," p. 612, Oxford Univ. Press (Clarendon), London/New York (1975).
16. F. GRONWOLD, H. HARALDSON, AND A. KJEKSHUS, *Acta. Chem. Scand.* **14,** 1879 (1960).
17. W. JEITSCHKO, *Acta Crystallogr. Sect. B* **30,** 2565 (1974).
18. W. H. ZACHARIASEN, *Acta Crystallogr.* **16,** 1253 (1963).
19. M. L. BUTLER, *J. Appl. Phys.* **48,** 1914 (1977).
20. S. R. MORRISON, "Electrochemistry at Semiconductor and Oxidized Metal Electrodes," Plenum, New York (1980).
21. J. C. W. FOLMER, J. A. TURNER, AND B. A. PARKINSON, *Inorg. Chem.* **24,** 4028 (1985).